J. Fluid Mech. (2000), *vol.* 420, *pp.* 301–324. Printed in the United Kingdom

Multiple solutions and flow limitation in collapsible channel flows

By X. Y. LUO[1] AND T. J. PEDLEY[2]

[1]Department of Mechanical Engineering, University of Sheffield, Sheffield S1 3JD, UK

[2]Department of Applied Mathematics and Theoretical Physics, University of Cambridge, Silver Street, Cambridge CB3 9EW, UK

(Received 15 October 1999 and in revised form 19 May 2000)

Steady and unsteady numerical simulations of two-dimensional flow in a collapsible channel were carried out to study the flow limitation which typically occurs when the upstream transmural pressure is held constant while flow rate and pressure gradient along the collapsible channel can vary independently. Multiple steady solutions are found for a range of upstream transmural pressures and Reynolds number using an arclength control method. The stability of these steady solutions is tested in order to check the correlation between flow limitation and self-excited oscillations (the latter being a consequence of unstable steady solutions). Both stable and unstable solutions are found when flow is limited. Self-excited oscillations and divergence instabilities are observed in certain solution branches. The instability of the steady solutions seems to depend on the unsteady boundary conditions used, i.e. on which parameters are allowed to vary. However, steady solutions associated with the solution branch before flow limitation where the membrane wall bulges are found to be stable for each of the three different boundary conditions employed. We conclude that there is no one to one correlation between the two phenomena in this two dimensional channel model.

1. Introduction

One of the questions of interest in the context of forced expiration from the lungs is whether there is a causal relationship between wheezing and 'flow limitation', i.e. the phenomenon that increasing a large expiratory driving pressure does not lead to an increase in flow rate on account of airway collapse. Gavriely *et al.* (1985, 1989) Gavriely & Grotberg (1988) and Grotberg & Gavriely (1989) sought to analyse the phenomenon by applying their flutter theory, developed for a parallel-sided channel, to a channel of slowly varying width, representing the narrowest part of the collapsed airway. Their results showed an encouraging agreement with a model experiment, and indicated that flow limitation is necessary but not sufficient for the onset of flutter. There are several other studies (Elliott & Dawson 1977; Webster *et al.* 1995; Carpenter & Garrad 1986; Carpenter & Morris 1990; Davies & Carpenter 1997*a*, *b*; Jensen 1990, 1992, 1998) on the same or similar systems, with a variety of different applications. All except Jensen's, however, have consisted of linear or nonlinear instability theories for flow in a long, *parallel-sided* channel, so in the basic state the steady flow is unidirectional and the elastic walls are planar.

There are a number of other physiological applications of flow in collapsible tubes. Examples are: arteries compressed by a sphygmomanometer cuff, intra-myocardial coronary blood vessels during systole, pulmonary blood vessels in the upper parts of

the lung, the urethra during micturition, and the glottis during phonation (Shapiro 1977; Kamm & Pedley 1989). Many laboratory experiments with model systems of collapsible tubes have revealed a rich variety of self-excited oscillations (Conrad 1969; Brower & Scholten 1975; Bonis & Ribreau 1978; Bertram 1986; Bertram & Castles 1999), some of which may be involved in wheezing. In these experiments either water or air flow has been studied in a segment of rubber tube. The observations have stimulated several theoretical studies aimed at understanding the mechanisms of the oscillations.

Many studies have been based on plausible but *ad hoc* one-dimensional models, which nevertheless may explain some of the observed phenomena (Shapiro 1977; Cancelli & Pedley 1985; Bertram & Pedley 1982; Jensen & Pedley 1989; Matsuzaki & Matsumoto 1989; Hayashi, Hayase & Kawamura 1998). However, such models cannot be rationally derived from the full governing equations, relying as they do on several *ad hoc* assumptions. Since 1994, a more realistic approach to the system has been made by Pedley and colleagues (Lowe & Pedley 1996; Rast 1995; Luo & Pedley 1995, 1996, 1998; Pedley & Luo 1998), using numerical simulations based on a two-dimensional model, i.e. flow in an asymmetric collapsible channel, where part of one wall of the channel is replaced by an elastic segment, and steady flow is assumed upstream. The elasticity of the segment can be described rationally, by treating it as a membrane which deforms subject to the hydrodynamic stresses, external pressure and longitudinal tension. Wall inertia, as well as fluid inertia, can be taken into account. This approach has provided a rational, yet feasible, description of an experimentally realizable system, although it is still some way from the full three-dimensional tube system. It has revealed a sequence of bifurcations, going through regular oscillations to irregular oscillations, showing several interesting dynamic features similar to those observed in the experiments. The important roles played by the membrane longitudinal tension and inertia, the energy loss in different parts of the flow domain, and the coupling between downstream vorticity waves and flow separation due to the channel collapse have been studied (Luo & Pedley 1995, 1996, 1998; Pedley & Luo 1998). Most of these studies, however, have been designed to correspond to one particular kind of experimental setup, in which the downstream transmural pressure (internal minus external pressure), P_{de}, is a control parameter. The so-called pressure drop limitation phenomenon (where the pressure drop does not continue to increase as flow rate increases, for large enough flow rate) is a common feature when P_{de} is held constant while the upstream pressure is varied, and is closely associated with the self-excited oscillations.

Flow limitation is a result of a different experimental scenario in which the upstream transmural pressure is controlled instead. This paper aims to simulate the flow limitation phenomenon in the two-dimensional model and investigate whether there is a causal link between the self-excited oscillations and flow limitation. This will be the first time that collapse and flutter have been examined together, self-consistently, in the same model problem. In contrast to most of the previous studies mentioned above, here the steady flow, from which the oscillations grow, involves a large deformation of the wall and separation of the flow (Luo & Pedley 1995, 1996).

In our previous studies, the flow rate and the downstream transmural pressure have been taken as given, and the pressure drop along the channel (hence the upstream transmural pressure) is the unknown. However, to investigate flow limitation it is necessary to fix the upstream transmural pressure and treat either the pressure drop or flow rate as an unknown. This computationally more challenging difficulty has been overcome in this paper by setting the reference pressure at the upstream end and

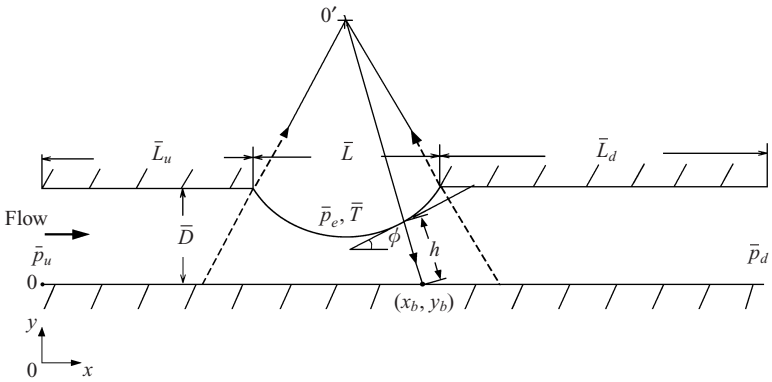

FIGURE 1. Two-dimensional flow configuration. Steady Poiseuille flow with average velocity $\overline{U}_0$ is assumed either at the entrance or exit, depending on which type of boundary condition is used. $\bar{p}_u = 0$ is the pressure at the upstream end, $\bar{p}_d = 0$ is pressure at the downstream end of the channel, $\bar{p}_e$ is the external pressure and $\overline{T}$ is the tension in the membrane. For explanation of other symbols, see text.

employing the arclength control method (Riks 1979; Heil 1997) so that the control parameters can be switched as required.

The two-dimensional model is briefly reviewed in § 2, and the numerical methods are discussed in § 3. Steady solutions for a range of parameters are given in § 4, including tests for stability of these solutions in § 4.3. A discussion is given in § 5, followed by conclusions in § 6.

2. The mathematical model

2.1. *Assumptions*

The flow configuration is shown in figure 1. The rigid channel has width $\overline{D}$; one part of the upper wall is replaced by an elastic membrane subjected to an external pressure $\overline{P}_e$. Steady Poiseuille flow with average velocity $\overline{U}_0$ is assumed either at the entrance or exit, depending on which type of boundary condition is used (see below); the fluid pressure at either the upstream or the downstream end is taken to be zero. The flow is incompressible and laminar, the fluid having density $\overline{\rho}$ and viscosity $\overline{\mu}$. The longitudinal tension $\overline{T}$ is taken to be constant, i.e. variations due to the wall shear stress or the overall change of the membrane length are considered to be small relative to the initial stretching tension. The assumption that membrane tension is constant in time was justified in a previous paper (Luo & Pedley 1996) through the demonstration that the length of the membrane varied by only 5% even during the most vigorous oscillations computed. In this paper the unsteady code is used principally to assess the stability of steady states to small-amplitude perturbations and to see whether an instability is divergent or oscillatory. Large-amplitude accuracy is not required so a constant length, and hence constant tension, is justified.

2.2. *Governing equations*

The dimensionless momentum and continuity equations are, in standard notation,

$$\frac{\partial u_i}{\partial t} + u_j u_{i,j} = -P_{,i} + \frac{1}{Re} u_{i,jj}, \tag{1}$$

$$u_{i,i} = 0, \qquad i = 1, 2, \tag{2}$$

where $Re = \overline{U}_0 \overline{D} \overline{\rho} / \overline{\mu}$ is the Reynolds number. The dimensionless membrane equation is

$$m \frac{\partial^2 \eta}{\partial t^2} - \kappa T + \sigma_n + P_e = 0, \tag{3}$$

where m is the ratio of the inertia of the membrane to the inertia of the fluid (see below), η is the displacement of the membrane in the normal direction, σ_n is the fluid stress acting on the membrane in the normal direction, P_e is the external pressure, T is the longitudinal tension, and κ is the wall curvature which can be expressed as the derivative along the membrane of the angle made by the tangent to the elastic boundary with the x-axis:

$$\kappa = \frac{\partial \phi}{\partial s}. \tag{4}$$

All the variables are non-dimensionalized as

$$\left.\begin{aligned} u_i = \overline{u}_i / \overline{U}_0 \quad (i = 1, 2), \quad \sigma = \overline{\sigma} / \overline{\rho}_f \overline{U}_0^2, \quad P = \overline{P} / \overline{\rho}_f \overline{U}_0^2, \quad T = \overline{T} / \overline{\rho}_f \overline{U}_0^2 \overline{D}, \\ x = \overline{x} / \overline{D}, \quad y = \overline{y} / \overline{D}, \quad \eta = \overline{\eta} / \overline{D}, \quad s = \overline{s} / \overline{D}, \quad t = \overline{t} \overline{U}_0 / \overline{D}, \quad m = \frac{\overline{\rho}_w \overline{w}}{\overline{\rho}_f \overline{D}}, \end{aligned}\right\} \tag{5}$$

where an overbar denotes dimensional variables; $\overline{\rho}_w$ and $\overline{\rho}_f$ are the densities of the membrane and fluid, respectively, and $\overline{w}$ denotes the thickness of the membrane, which is taken to be much smaller than the channel width $\overline{D}$.

2.3. *Boundary and initial conditions*

The definition of the boundary conditions depends on the control parameters chosen. In this simple mathematical model, the following control parameters can be varied, as they can in the analogous experiments: the upstream transmural pressure $P_{ue} = P_u - P_e$, the downstream transmural pressure $P_{de} = P_d - P_e$, the longitudinal tension T, and the flow rate. As the fluid viscosity and density are fixed, to correspond to water, a change in flow rate is equivalent to a change of Re. Thus in the following, we will use Re, instead of flow rate, as the control parameter.

For given constant tension T, one can specify any two control parameters among P_{ue}, P_{de}, and Re, and calculate the remaining one from the equations. In this paper, the following three boundary conditions are used:

BC(I): $P_{ref} = P_u = 0$, P_{ue}, P_{de} given, and Re unknown
Inlet flow: $\sigma_n \simeq -P_u = 0$, $\sigma_t = 0$ at $x = 0$, $0 \leqslant y \leqslant 1$,
Outflow: $\sigma_n \simeq -P_d$, $v = 0$ at $x = L_u + L + L_d$, $0 \leqslant y \leqslant 1$,
Elastic wall: $P_e = -P_{ue}$.

BC(II): $P_{ref} = P_u = 0$, P_{ue}, Re given, and P_{de} unknown
Inlet flow: $\sigma_n \simeq -P_u = 0$, $\sigma_t = 0$ at $x = 0$, $0 \leqslant y \leqslant 1$,
Outflow: $u = 6y(1 - y)$, $v = 0$ at $x = L_u + L + L_d$, $0 \leqslant y \leqslant 1$,
Elastic wall: $P_e = -P_{ue}$.

and

BC(III): $P_{ref} = P_d = 0$, P_{de}, Re given, and P_{ue} unknown:
Inlet flow: $u = 6y(1 - y)$, $v = 0$ at $x = 0$, $0 \leqslant y \leqslant 1$,
Outflow: $\sigma_n = 0$, $\sigma_t = 0$, at $x = L_u + L + L_d$, $0 \leqslant y \leqslant 1$,
Elastic wall: $P_e = -P_{de}$.

All these cases have the same boundary conditions on the walls:

$$\text{Rigid walls:} \quad u = v = 0 \quad \text{at} \quad y = 0,\ 0 \leqslant x \leqslant L_u + L + L_d$$
$$\text{at} \quad y = 1,\ 0 \leqslant x \leqslant L_u \text{ and } L_u + L \leqslant x \leqslant L_u + L + L_d.$$

$$\text{Elastic section:} \quad u(t) = u_w(t), \quad v(t) = v_w(t) \quad \text{at} \quad x = x_w(t),\ y = y_w(t),$$

where, on the elastic section, x_w and y_w are the membrane coordinates of a general point on the wall, which are updated during the computation using the method of spines (Luo & Pedley 1996).

In our previous internal fluid flow computations, the pressure at the flow outlet has been chosen as reference pressure; hence the downstream transmural pressure becomes a constant for a given external pressure P_e. This is equivalent to BC(III). Such a choice is not very convenient for the present study, since it is the upstream, not the downstream, transmural pressure that needs to be held constant. One way to hold the upstream transmural pressure constant is to adjust the upstream and external pressures during the computations (Luo & Pedley 1998), as is done in some experiments (C. D. Bertram, private communication). However, such an approach slows down the iteration procedure and sometimes causes divergence if the pressure changes are large.

An alternative way to hold the upstream transmural pressure constant is to choose the reference pressure (to be zero) at the flow inlet, so that the upstream transmural pressure is a constant for a given external pressure. This has a great advantage since we can control either the downstream pressure as in BC(I) or flow rate (Re) as in BC(II) while keeping the upstream transmural pressure constant during the iterations. In this paper, therefore, boundary conditions BC(I) and BC(II) are used to calculate the steady solutions.

Obviously, for the same control parameters, identical steady solutions should be obtained from BC(I), BC(II), or BC(III). Thus in the time-dependent computations performed to test the instability of the steady solutions, any of the three boundary conditions may be used. The unsteady solutions, however, do depend on which of the three boundary conditions is used, as is shown later.

For every time-dependent computation, the initial condition was taken to be the computed steady state with a small perturbation on one of the control parameters. Therefore, one can determine the stabilities of the steady solution by the growth or decay of the corresponding perturbations in the system (Luo & Pedley 1996).

2.4. *Parameters*

The parameter values used are as follows:

$L_u = 5, \quad L = 5, \quad L_d = 30,$

$T = T_0/\beta = 1.610245 \times 10^7/Re^2\beta, \ P_{ue} = 0\text{–}1 \times 10^5/Re^2,$

$Re = 1\text{–}1000,$

where β is a parameter ($\geqslant 1$) used to vary the value of tension. Typically, the value of β is chosen between 10 and 35. All the parameters are chosen to be the same as or close to the values used in the previous studies (Luo & Pedley 1995, 1996, 1998). The effects of wall inertia on this system have been illustrated in a previous paper (Luo & Pedley 1998), so m is chosen to be zero in this study, for simplicity.

The dimensionless pressure (and tension) depend on Re because of the non-dimensionalization used in § 2.2. To present a relation between the flow rate (Re) and the pressure drop, for fixed dimensional $\overline{P}_{ue}$ and tension, as in an experiment, we need to rescale the results from the Navier–Stokes equations. Thus the new non-

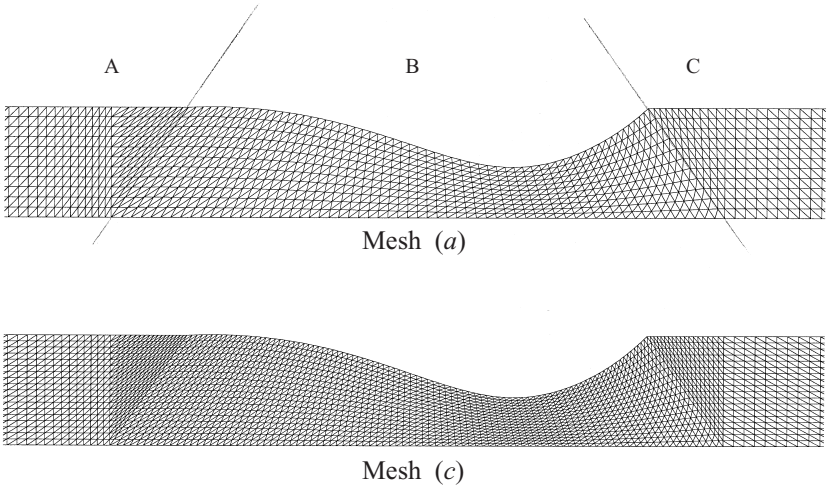

FIGURE 2. Part of a typical adaptive mesh of the flow domain. Mesh (*a*): there are 5060 triangular elements and 10 603 nodes, with 2875 movable nodes located in section B; mesh (*c*): 200% refined mesh with 19 647 nodes and 9540 elements, including 6845 movable nodes located in section B.

dimensional pressure and tension P^*, T^* are: $P^* = P \times Re^2$, $T^* = T \times Re^2$, where P and T are the non-dimensional pressure and tension defined in § 2.2. Obviously, P^* and T^* are now proportional to the physical pressure and tension. In the following the star will be dropped for simplicity.

3. Methods

3.1. *Adaptive moving mesh and time integration*

The methods used to solve the steady and unsteady problems have been described in detail in previous papers (Rast 1994; Luo & Pedley 1996, 1998), where a simultaneous approach is employed, i.e. the fluid and wall motions are computed together. The movable mesh is made adaptive by using the method of spines in a mixed Lagrangian–Eulerian reference frame (Rast 1994; Siliman 1979; Ruschak 1980; Saito & Scriven 1981). A second-order predictor-corrector difference scheme with a variable time increment controlled by the error tolerance is used to solve the time-dependent coupling problem (Gresho, Lee & Sani 1979).

The flow domain is divided into three six-node triangular finite element subdomains (figure 2). Subdomains A and C have nodes fixed in space, while subdomain B, under the elastic section, contains the mesh with moving nodes.

The elemental nodes under the elastic section lie along the spines which emanate from a fixed origin O_s. Each spine k is defined by the Cartesian coordinates of its base point, x_b^k and $y_b^k (= 0)$, and the direction from that point to the origin. The position of node i on spine k is given in terms of a fixed fraction ω_i^k of the spine height h^k as

$$x_i^k = x_b^k + \alpha_x^k \omega_i^k h^k, \tag{6}$$

$$y_i^k = y_b^k + \alpha_y^k \omega_i^k h^k, \tag{7}$$

where $\boldsymbol{\alpha} = (\alpha_x^k, \alpha_y^k)$ is the direction vector of spine k, and the spine height is simply the

distance from the spine base to the elastic surface in the direction of $\boldsymbol{\alpha}$. Each spine height is an unknown in the problem and is to be determined as part of the solution.

The variables are as usual expanded isoparametrically in area coordinates, (ζ, η), employing a mixed interpolation, with u, v, x, and y sharing quadratic and P linear expansions:

$$u = \sum_{i=1}^{6} u_i N_i(\zeta, \eta), \quad v = \sum_{i=1}^{6} v_i N_i(\zeta, \eta), \quad P = \sum_{i=1}^{3} P_i L_i(\zeta, \eta), \tag{8}$$

$$x = \sum_{i=1}^{6} x_i(h, \theta) N_i(\zeta, \eta), \quad y = \sum_{i=1}^{6} y_i(h, \theta) N_i(\zeta, \eta), \tag{9}$$

where L_i and N_i are linear and quadratic shape functions respectively, and θ is the angle of a spine with the vertical (Rast 1994). Boundary elements are oriented so that three nodes ($l = 3$, 5 and 2) lie along the elastic membrane. The coordinates of all nodes below the elastic boundary depend on the boundary position, therefore ϕ, $\hat{\boldsymbol{n}}$, ds, and the Jacobian of the coordinate transformation for those elements which contain these nodes, are all functions of x and y, hence of the spine height h.

The global finite element matrix equation

$$\boldsymbol{M}\frac{\mathrm{d}\boldsymbol{U}}{\mathrm{d}t} + \boldsymbol{K}(\boldsymbol{U})\boldsymbol{U} - \boldsymbol{F} = \boldsymbol{R}, \tag{10}$$

where $\boldsymbol{U} = \{u, v, P, h\}$, assembled using the frontal technique, is solved with a second-order predictor-corrector time integration scheme with variable time increment and Newton–Raphson iteration. A small value of ϵ (between 10^{-5} and 10^{-7}) is chosen as both the convergence criterion for the Newton–Raphson iterations and the tolerance for the time-truncation error (Luo & Pedley 1996).

3.2. *Computational accuracy*

Although the accuracy of the current code was thoroughly tested in our previous studies, further tests are required since we are exploring a new region of parameter space. Accuracy was tested by using three different meshes. Mesh (*a*) (figure 2) is a typical grid used in the previous studies and has 5060 six-node triangular elements and 10 603 nodes, with 2829 movable nodes (682 elements) located in section B. This grid was found to be satisfactory with and without wall inertia (Luo & Pedley 1998), for Reynolds number up to 500 (Luo & Pedley 1995). Mesh (*b*) is a refined mesh which has 16 415 nodes and 7956 elements. Mesh (*c*) (figure 2) is a still more refined mesh which has 19 649 nodes and 9540 elements, an increase of nearly 100% in element numbers.

Results obtained from the three different meshes are shown in figure 3, where Re versus P_{ud} is plotted for $\beta = 35$, $P_{ue} = 0.896 \times 10^5$. It is clear that using mesh (*a*) led to incorrect results in the upper branch where Re is higher. This means that mesh (*a*) does not have enough grid points for the parameter space investigated. It is noted that the results from all three meshes agree very well for $Re < 570$, which is consistent with our previous tests with mesh (*a*) for $Re < 500$. The results for meshes (*b*) and (*c*) do not differ significantly from those of mesh (*a*) along the lower solution branch, even when $Re > 570$. This is because the corresponding wall configurations along this branch are fully or partially collapsed, in contrast to the upper-branch cases for which the membranes bulge out. A collapsed wall shape means an automatically refined mesh along the y-axis since we use same number of nodes along each spine. As the

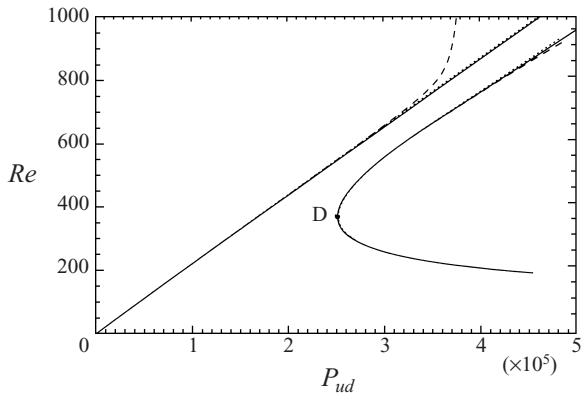

FIGURE 3. Results for steady calculated flow using mesh (*a*) (dashed line), mesh (*b*) (dotted line), and mesh (*c*) (solid line). In the upper branch where *Re* is higher, results from mesh (*a*) is deviating from those of mesh (*b*) and (*c*). All results are obtained using BC(II).

differences between mesh (*b*) and (*c*) is less than 1% and we are mainly interested in the lower branch of solutions, mesh (*b*) was chosen in the current study.

3.3. *Arclength control*

An inappropriate choice of the control parameter can sometimes cause the numerical scheme to break down, especially if multiplicity of solutions exists. In our case, once T and P_{ue} are fixed, there are two control parameters, Re and $P_{ud} = P_u - P_d$. If the solution curve is monotonic in the Re, P_{ud} space, then either control parameter can be used to obtain a solution. However, problems occur if the solution curves are non-monotonic. In a previous study, we tried to obtain a flow limitation curve in Re, P_{ud} space and found that solutions were not attainable as the pressure drop is reduced beyond a critical value (Figure 18, Luo & Pedley 1998). Without knowledge of what the solution curve should be, we speculated that the breakdown of the solution was possibly due to a numerical instability. In the present study, in which we follow the incremental approach, or arclength methods, that have been developed for snap-through and buckling problems in solid mechanics (Riks 1979; Heil 1997), we find that the breakdown point in figure 18 of Luo & Pedley (1998), is actually a turning point (critical point), and the solution becomes multiple valued, as at point D in figure 3.

To build up an efficient arclength control scheme requiring no manual interventions, we relate the switch of the control parameters along the arclength of the solution curve with the number of iterations required for one solution during the calculations. We start with one initial control parameter, and increase it incrementally. If a solution is obtained within four iterations, which indicates a slow change of arclength in the direction of this control parameter, then the control parameter is increased along the arclength. On the other hand, if convergence is achieved after more than eight iterations, indicating a rapid change of arclength, then the control parameter is decreased. Further, if the increment of the control parameter becomes too small, indicating a possible turning point of the curve (or very fast change in this direction), then the procedure is switched to the other control parameter. Whether to increase or decrease the new control parameter depends on the direction of the arclength calculated before the switch, see figure 4.

It should be noted that whenever the control parameter is switched, the boundary conditions change accordingly from BC(I) to BC(II) (see § 2.3) or vice versa. This

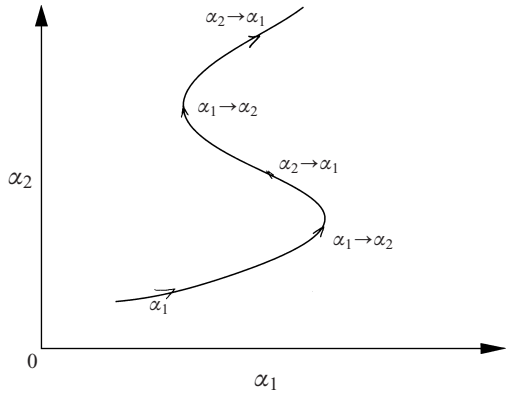

FIGURE 4. The increase/decrease and switch of control parameters α_1 and α_2 are determined by the convergence rate.

requires a perfect match of results from the two sets of boundary conditions. One hidden problem is that for BC(II), the parabolic velocity inlet profile can be easily specified since the flow rate (*Re*) is known. For BC(I), however, *Re* is an unknown, only pressures being specified. In this case, a scale Reynolds number is used in the equations, and the actual Reynolds number is calculated as the product of the scale Reynolds number and the computed inlet average velocity. However, the computed velocity profile at the inlet would not be parabolic unless special precautions were taken, and then the average velocity would have to be obtained by integrating the velocity across the channel. The numerical error of this integration is increased when the parameter is switched. Therefore small jumps can occur. The jumps can be crucial when a sharp corner in the solution curve is encountered. To overcome this problem, we modify the boundary condition BC(I) so that the unknown is chosen to be the velocity at the middle element of the inlet cross-section, u_{max}; at the rest of the element nodes, the velocities in the x-direction are related to u_{max} by imposing a parabolic profile. Hence, the pressure can be specified while a parabolic velocity profile is ensured and no integration is needed to calculate *Re*. After this treatment, the solution curves became much smoother whenever the control parameter was switched, and even sharp corners can be captured automatically (see figure 5).

4. Results

4.1. *Steady solutions at* $\beta = 35$

For a set of given values of the upstream transmural pressure P_{ue}, and a fixed tension, we have calculated the steady solutions in the Re, P_{ud} space for $0 < Re \leqslant 1000$, and $0 < P_{ud} \leqslant 4.8 \times 10^5$. Figure 5 shows all the steady solutions when $\beta = 35$ and $P_{ue} = (-0.4 \text{ to } 0.896) \times 10^5$. Solutions for other values of β are found to have similar behaviour, and will be discussed later. The solution for Poiseuille flow when the elastic wall is undeformed is also shown as the dashed line in figure 5. It can be seen that for $P_{ue} = -0.4 \times 10^5$ to 0.4×10^5, the flow rate increases at the beginning with the driving pressure difference P_{ud}, as in Poiseuille flow, indicating that the channel is only gently collapsed, if at all. However, as the driving pressure increases, i.e. the downstream suction increases, the transmural pressure across the membrane becomes more and more negative, and the membrane becomes increasingly collapsed, therefore

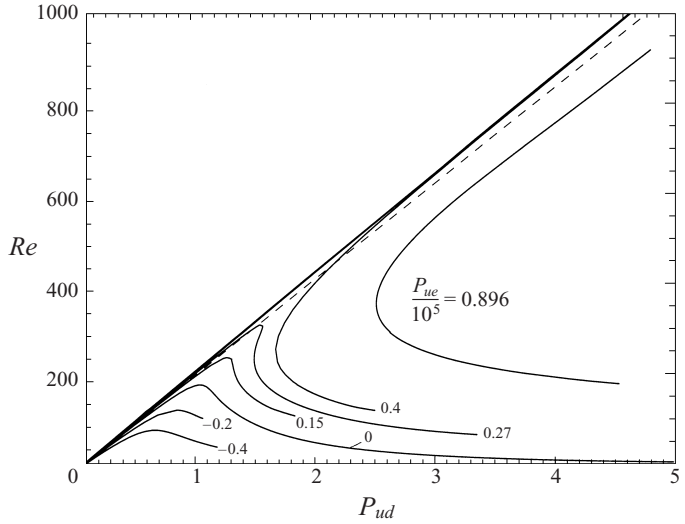

FIGURE 5. Steady solutions obtained for $\beta = 35$, and $P_{ue}/10^5 = -0.4$, -0.2, 0, 0.15, 0.27, 0.4, and 0.896. The dashed line indicates the results obtained from the Poiseuille flow in the undeformed channel.

increasing the flow resistance. The flow rate is thus limited for large enough driving pressure (e.g. $P_{ud} > 1.1 \times 10^5$ when $P_{ue} = 0$). Once the flow rate reaches its peak value, it decreases as P_{ud} increases; in the context of forced expiration, this is known as 'negative effort dependence' (Hyatt, Schilder & Fry 1958). The lower the upstream transmural pressure, the smaller is the flow rate at which flow is limited.

It is interesting to note that, for $P_{ue} = 0.15 \times 10^5$, the slope of the curve after the flow limitation is almost vertical. For $P_{ue} > 0.15 \times 10^5$, there is a limit point and the curve starts to turn backwards. Thus there are multiple solutions at given P_{ud}, as well as given Re, presenting a hysteresis similar to the snap-through behaviour of a shallow tied arch (Thompson & Hunt 1973). In dynamical system terms, this looks analogous to a saddle-node, or cusp bifurcation. As P_{ue} is further increased, the limit point moves rapidly up the first branch, and looks as if it is going to infinity, which would represent a second bifurcation, when $P_{ue} \approx 0.4 \times 10^5$. The curve appears to split into two branches. One of these is almost parallel to the curve for Poiseuille flow, represents a fully bulged wall shape (see below) and no flow limitation occurs; the other has an upper branch which is also nearly parallel to the first and represents partially collapsed and partially budged wall shape, and a lower branch which exhibits negative effort dependence and a fully collapsed wall shape. Hence, for a given driving pressure, there exist three different steady flow rates.

To understand these results more fully, we now examine particular cases in more detail.

Case A: $P_{ue} = 0$

Figure 6 shows the wall shapes and solutions curves for $P_{ue} = 0$. For this case, the transmural pressure along the membrane remains less than zero for all the values of Re and P_{ud}, and the wall configurations remain collapsed (i.e. $y_w < 1$) everywhere. The maximum Reynolds number is less than 200. The dashed curve in figure 6(a) represents the wall shape for the maximum Reynolds number at point * ($Re = 191$). Points A_1 ($Re = 102$) and A_2 ($Re = 125$) are two different solutions located on

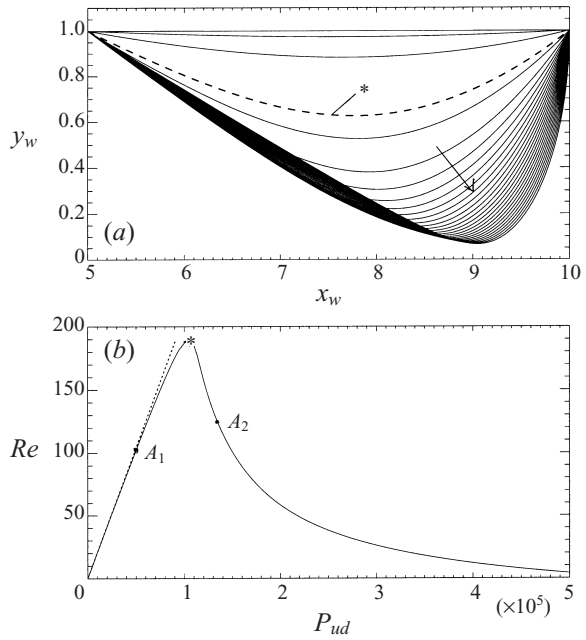

FIGURE 6. Case A: (*a*) wall shapes and (*b*) Re, P_{ud} curve: $\beta = 35$, $P_{ue} = 0$. The dashed line in (*a*) corresponds to the turning point * in (*b*), and the dotted line in (*b*) represents the solutions from the Poiseuille flow in the undeformed channel. The arrow in (*a*) indicates the direction of increasing P_{ud}.

different branches of the solution curve (one of which represents flow limitation), whose stability will be considered later. These results indicate a fold bifurcation at the turning point *.

Case B: $P_{ue} = 0.27 \times 10^5$

The wall shapes for $P_{ue} = 0.27 \times 10^5$ are plotted in figure 7(*a*). In this case, the upstream transmural pressure is positive, and the initial wall shape when the flow rate is small is therefore a bulged configuration, as shown by the dotted curve 0. As the flow rate increases, the transmural pressure at the downstream end decreases, so the membrane is sucked in from its bulged shape into a collapsed one. The turning point * occurs just after the membrane starts to collapse, the corresponding wall shape being the dashed curve in figure 7(*a*); thereafter, the degree of collapse increases. Not only does the flow rate decrease after it is limited, but the driving pressure decreases too at first and then increases again. This hysteresis response gives rise to three different solutions at one driving pressure (see figure 7). Points B_1 ($Re = 303$), B_2 ($Re = 270$), and B_3 ($Re = 220$) represent the three solutions at a single driving pressure, $P_{ud} = 1.5 \times 10^5$, and the curve * ($Re = 319$) is at the turning point. The solution curve here resembles a cusp bifurcation.

Case C: $P_{ue} = 0.4 \times 10^5$

This is an extreme hysteresis case for which the first turning point has moved to large *Re*. The solution curve is interesting in that the upper and lower solution branches almost overlap for $P_{ud} > 2.5 \times 10^5$. In figure 8(*b*), the solutions at C_5, C_5' are virtually identical in Re, P_{ud} space, but the wall shapes are quite different, see dash-dotted curves in figure 8(*b*). As *Re* increases from point 0 ($Re = 1$) to C_1 ($Re = 434$), the wall shape

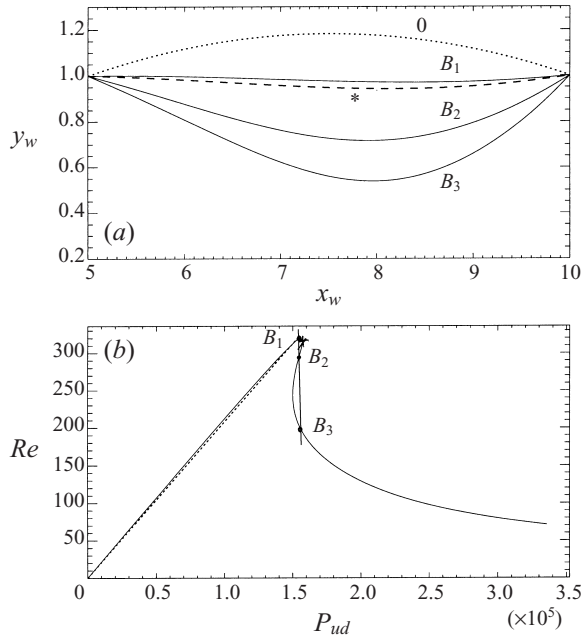

FIGURE 7. Case B: (*a*) wall shapes and (*b*) Re, P_{ud} curve: $\beta = 35$, $P_{ue} = 0.27 \times 10^5$. The dotted line in (*a*) is the wall shape at $Re = 1$, point 0 in (*b*); B_1, B_2, B_3 are the three solutions at the same driving pressure; and the dashed line represents the wall shape at the turning point *.

remains bulged but the extend of bulging is decreased. From C_1 to C_5 ($Re = 869$), the wall shape does not change much, but from C_5 upwards to * ($Re = 1308$), where the curve turns, the downstream part of the wall increasingly bulges out again, and the maximum bulging point moves further downstream. Back from * to C_2 ($Re = 410$), where the two curves start to diverge, the wall gradually becomes almost undeformed as the curve crosses over the Poiseuille solution (dotted line in figure 8*c*). Once the curve turns around the corner C_4, the membrane collapses increasingly. Points C_1, C_2, and C_3 ($Re = 158$) represent three solutions at one value of $P_{ud}(= 2 \times 10^5)$. Unlike the previous cases, here the wall shape remains bulged as the flow is first limited at the point *. It should be noted that the solution at the turning point * is unlikely to be accurate with the current numerical resolution, since $Re > 1000$. However, the fact that there exists a turning point is very important, as it clearly indicates that after the cusp forms, the bifurcation seems to have moved to infinity.

Case D: $P_{ue} = 0.896 \times 10^5$

As P_{ue} is further increased to 0.896×10^5, the limit point has moved far to the right, and the solution appears to split into two distinct branches, as shown in figure 5 and figure 9(*b*). The first branch starts from zero and increases monotonically through point D_4' ($Re = 500$) and D_1 ($Re = 950$), and represents an entirely bulged wall shape. The second one has an upper part from * ($Re = 364$) to D_2 ($Re = 844$), and a lower part from * to D_3 ($Re = 180$). In the upper part of the second branch, solutions are associated with a wall shape in which a large upstream portion bulges out, but the downstream part remains collapsed. The lower part of the second branch is the flow limitation phase, with most of the membrane collapsed except at the very upstream end where the there is a slight bulge. The three different solutions at one given $P_{ud}(= 4.5 \times 10^5)$ are shown as wall shapes D_1, D_2, D_3 (solid curves) in figure 9(*a*). The

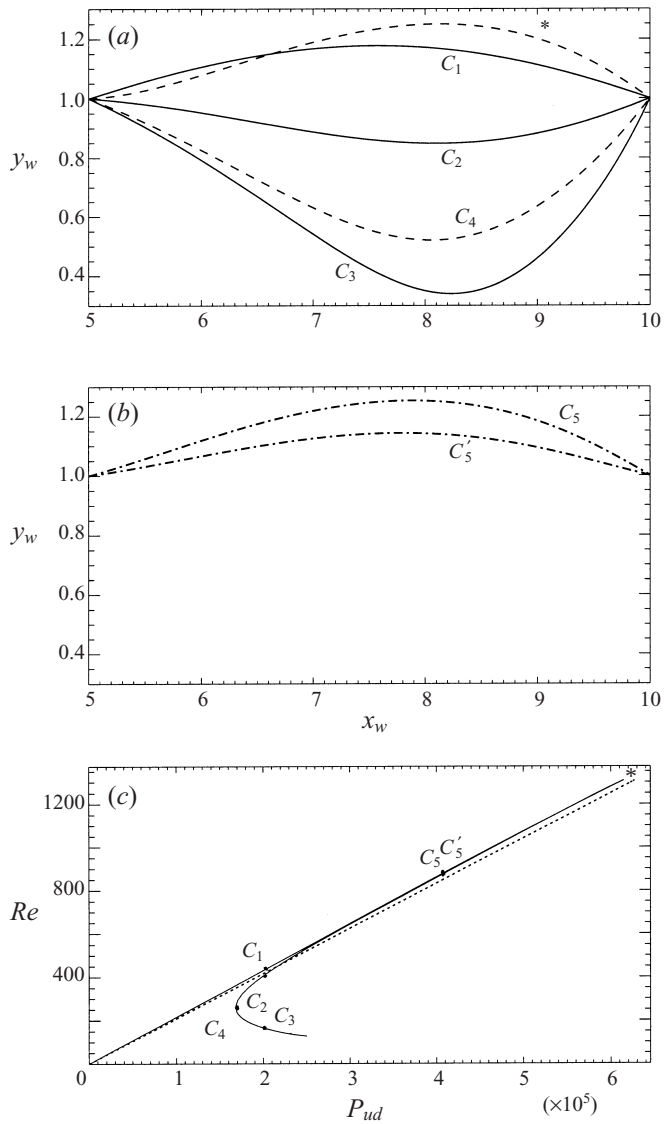

FIGURE 8. Case C: (a, b) wall shapes and (c) Re, P_{ud} curve: $\beta = 35$, $P_{ue} = 0.4 \times 10^5$. The three solid lines in (a) are the three solutions C_1, C_2, and C_3 at the same driving pressure. * is the upper turning point (upper dashed line in a), and C_4 is the lower turning point (lower dashed line in a). The dash-dotted lines in (b) are solutions for points C_5 and C_5', which are overlapped in (c). The dotted line in (c) represents the Poiseuille flow in the undeformed channel.

dashed curve is the solution at the turning point *. Point D_5 ($Re = 300$) is marked in figure 9(b), as it is known to be a solution which when perturbed will give rise to self-excited oscillations (Luo & Pedley 1997). Point D_4 ($Re = 500$) is another solution which we will look at later.

Figure 10 shows the streamlines for three different solutions, marked in figure 9(b) as D_2, *, and D_3. It can be seen that as the wall is partially bulged and partially collapsed at point D_2, two separation zones exist. As Re decreases, the membrane becomes more and more collapsed, the bulging separation disappears and the collapsing separation

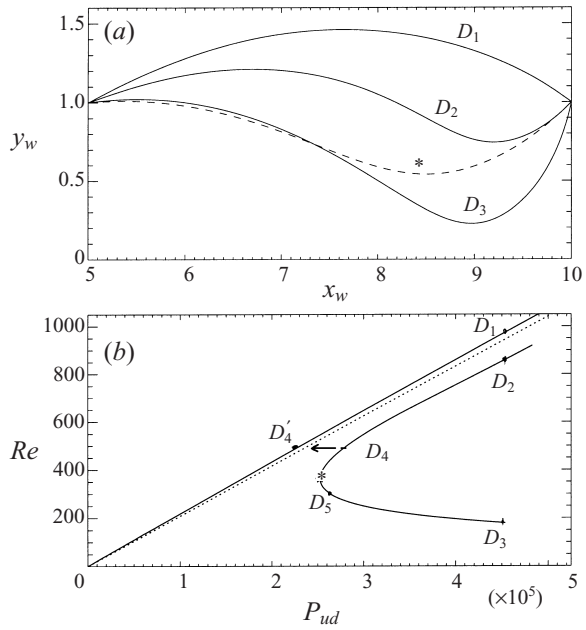

FIGURE 9. Case D: (*a*) wall shapes and (*b*) Re, P_{ud} curve: $\beta = 35$, $P_{ue} = 0.896 \times 10^5$. The thin dashed line in (*a*) is the wall shape at the turning point, * in (*b*). Points D_1, D_2, D_3 are the three multiple solutions at the same driving pressure.

is enlarged. As the curve in figure 9(*b*) turns over and becomes flow limited, the size of the primary separation remains more or less unchanged, but a secondary separation zone appears at the opposite wall. The variation of the flow separation zones is best shown in figure 11, where the stars represent the flow separation, and the triangles indicate the flow reattachment. These are calculated from the zero shear stress point at the upper wall. It is shown that for $Re \geqslant 680$, there are two separation zones, one upstream ($x_w \leqslant 5$) due to the upstream membrane bulging and one downstream due to the collapse of the elastic section ($x_w \geqslant 8$). For Re below 680, only one separation zone at the downstream is found as the membrane is almost fully collapsed, see figure 9.

4.2. *Steady solutions at higher values of tension*

It looks as if the value of the upstream transmural pressure P_{ue} is crucial in obtaining the bifurcated solution branches such as those in Case D for a given value of β (tension). Up to now, we have only looked at a single value of tension, $\beta = 35$. It is of interest to see what happens if different values are used, especially large values since smaller ones cause the membrane at the downstream end to be sucked into the rigid channel and the numerical code breaks down (Luo & Pedley 1996). Figure 12 shows that when $\beta = 25$ and 30 respectively, the solutions look very similar. Note that a slightly different value of P_{ue} is used in figure 12 for $\beta = 25$. This is because we want to include the solutions marked as points E_1, E_2 in the solution curves, of which again we know the stability behaviour from a previous study (Luo & Pedley 1996).

It is clear that, if tension is very high, the whole system will behave just like flow in a rigid channel. The solution curve will be similar to that for Poiseuille flow. However, as tension decreases, bifurcation occurs. We found that, for $P_{ue} = 0.27 \times 10^5$,

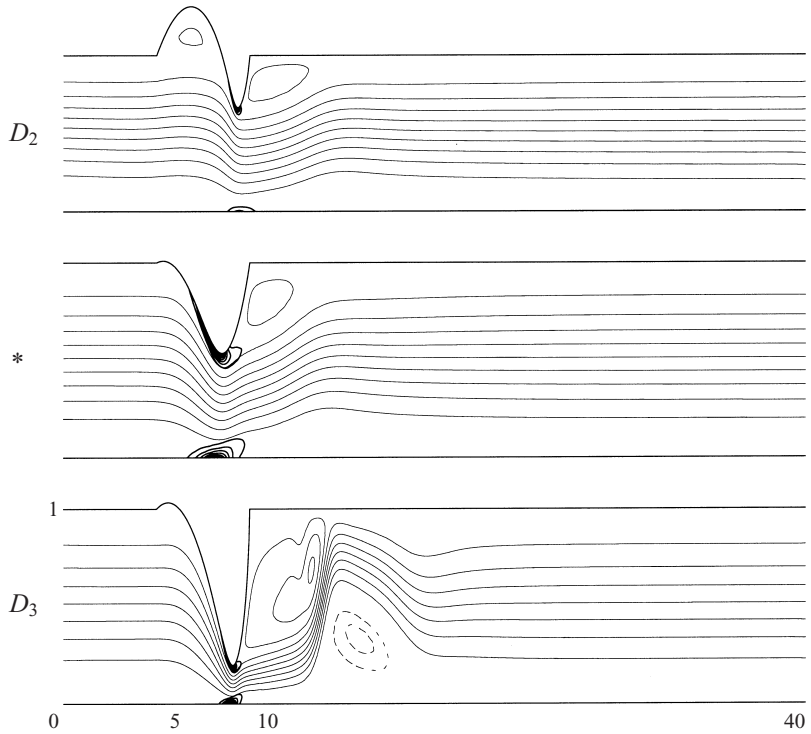

FIGURE 10. Streamlines at points D_2, *, D_3, on the lower branch of the curve in Case D. Solid streamlines are drawn with equal intervals between neighbouring values, except one which is 0.985 times the maximum value of the stream functions. Dotted line indicate streamlines of negative value, and are 0.6 and 0.9 times of the minimum value of the stream functions, respectively. Darker lines are ten equal spaced contours of energy dissipation to be discussed in § 5.

as tension is decreased from $\beta = 1$ to about $\beta = 3.5$, multiple solutions appear. For higher tension, no flow limitation occurs for $Re \leqslant 1000$. Results from the different values of β for $P_{ue} = 0.27 \times 10^5$ are shown in figure 13. Though not simulated directly, one can expect that the system would experience the cusp bifurcation which moves rapidly to large Re as tension is reduced from $\beta = 1$ to $\beta = 35$ for $P_{ue} = 0.896 \times 10^5$, as happens when P_{ue} is increased for a constant β (=35) in figure 5. Thus tension also plays an important role in generating a multiplicity of solutions in the system.

4.3. *Stability of the steady solutions*

To investigate the stability of all the steady solutions obtained in the previous section is not possible with our numerical approach, as extensive unsteady computation is involved when each steady solution is perturbed. Instead, we will select some solutions located on different solution branches and hope to find whether there is a correlation between the appearance of instability and the occurrence of flow limitation. To investigate the stability of these solutions, we can either perturb the initial condition (by choosing a slightly different steady solution adjacent to the one to be tested), or perturb the boundary conditions (by perturbing pressure on the elastic wall, say) for a short time, and run the unsteady code to see if the disturbances vanish in time. Sometimes, no perturbations need to be introduced, as the numerical error in the code, however small, is enough to trigger unstable behaviour.

One important feature, however, is that the unsteady results may depend on which

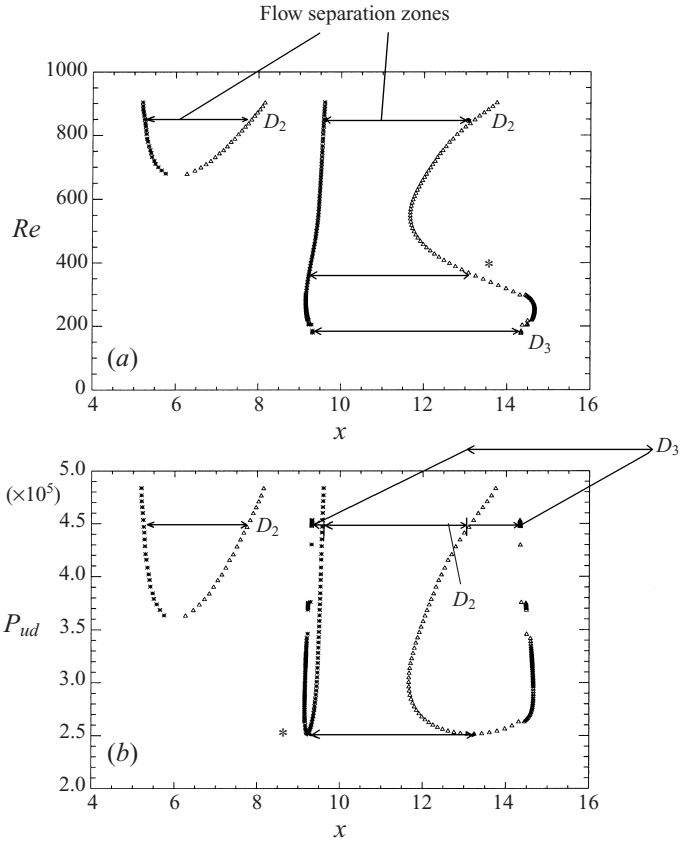

FIGURE 11. Flow separation zones of flow domain for Case D. The asterisks represent the values of x at which the flow separates and the triangles indicate the values of x at which it reattaches, plotted against Re (*a*) and P_{ud} (*b*). The points D_2, D_3 and * can be found in figure 9.

type of boundary condition is chosen (see § 2.3). This is certainly true for finite-amplitude disturbances in a rigid channel (Pugh & Saffman 1988; Barkley 1990). To perturb the steady solution using an unsteady calculation, one approach is to choose the downstream pressure to be zero, fix the upstream flow rate (Re), and calculate the upstream pressure (BC(III)), as we did in the previous studies; the second approach is to choose the upstream pressure to be zero, fix the downstream flow rate (Re), and calculate the downstream pressure (which will be negative) (BC(II)); or thirdly choose the upstream pressure to be zero and calculate Re for a given downstream (negative) pressure (BC(I)). Any of these approaches may be realized in a carefully controlled experiment (although in an experiment, it is often difficult to control the parameters in the way envisaged here: C. D. Bertram, personal communication).

It is found that all three boundary conditions indeed yield the same steady solutions; solution curves obtained in the current study (using BC(I) and BC(II)) pass through the solutions D_5 (figure 9), E_1, and E_2 (figure 12), obtained in the previous studies (using BC(III)), for example. The results of perturbing one steady solution with the three different boundary conditions mentioned in § 2.3 are shown in table 1, which lists results for selected points from the previous cases. Points A_1, A_2, are chosen from Case A in figure 6, and points B_1, B_2, B_3 are from Case B, and so forth.

In table 1, when the solution is marked unstable, it means that the unsteady

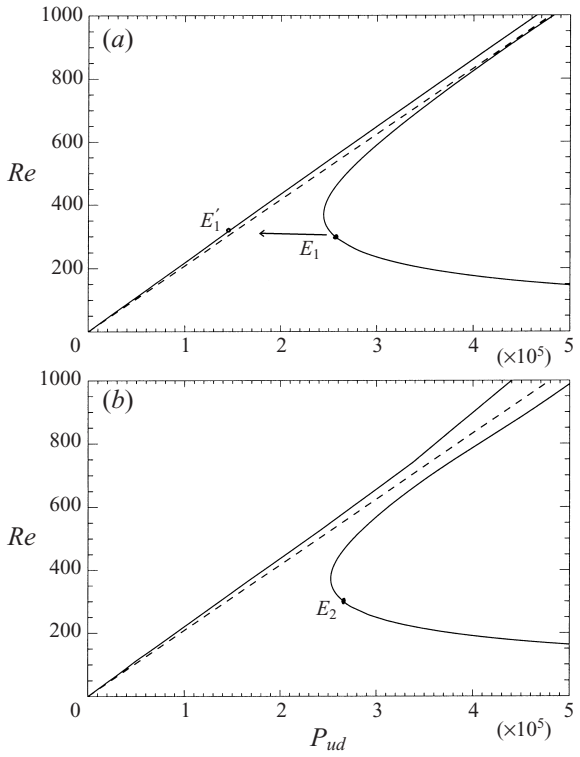

FIGURE 12. Re, P_{ud} curve for (*a*) $\beta = 25$, $P_{ue} = 0.8 \times 10^5$, and (*b*) $\beta = 30$, $P_{ue} = 0.896 \times 10^5$. The dashed lines represent the Poiseuille flow in an undeformed channel. E_1 is a stable solution when fixing the downstream transmural pressure, and E_2 is an unstable solution.

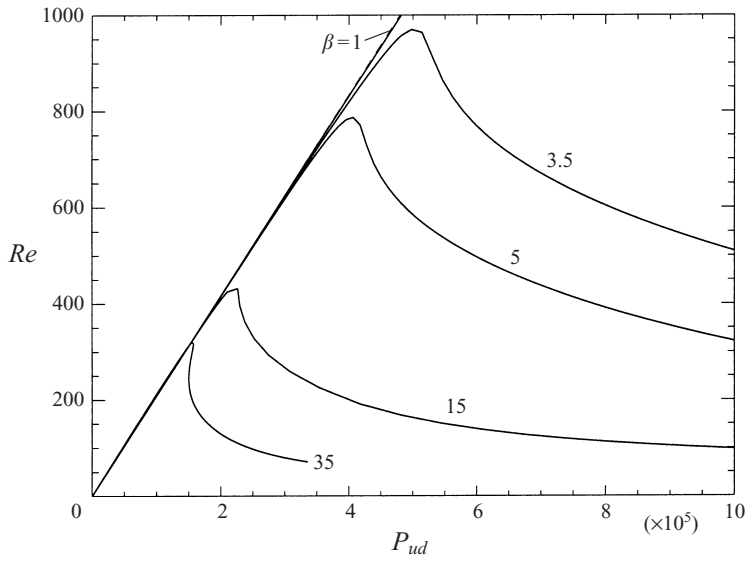

FIGURE 13. Re, P_{ud} curve for different values of β, and $P_{ue} = 0.27 \times 10^5$, showing that tension is important for the bifurcation to occur. The dashed line represents the Poiseuille flow and is almost indistinguishable from the curve for $\beta = 1$.

Solution point	BC(I)	BC(II)	BC(III)
A_1	stable	stable	stable
A_2	unstable	unstable	stable
B_1	stable	stable	stable
B_2	unstable	unstable	unstable*
B_3	unstable	unstable	unstable*
B_4	unstable	unstable	unstable*
C_1	stable	stable	stable
C_2	unstable	unstable	unstable*
C_3	unstable	unstable	stable
C_5	stable	stable	stable
C_5'	unstable	unstable	unstable*
D_1	stable	stable	stable
D_2	unstable	unstable	unstable*
D_3	unstable	unstable	unstable*
D_4	unstable	unstable	unstable
D_4'	stable	stable	stable
D_5	unstable*	unstable	unstable*
E_1	unstable	unstable	stable
E_2	unstable	unstable	unstable*

TABLE 1. Stability test of selected points from the solution curves. Here unstable* means the solution presents self-excited oscillations in the time period investigated. The three boundary conditions are BC(I): P_{ue}, P_{de} given, Re unknown; BC(II): P_{ue}, Re given, P_{de} unknown; and BC(III): P_{de}, Re given, P_{ue} unknown.

solution does not approach to the steady one in the time period investigated. There are three scenarios once the steady solution is perturbed. One is that the system clearly presents a divergence instability, and the unsteady solution may then be attracted to another (stable) steady solution at the same value of Re or P_{ue}, depending on which boundary condition is used. For example, point D_4 is found to be unstable, but converges to D_4', see figure 9. The other scenario is that self-excited oscillations set in immediately after the perturbation, and those cases are indicated by unstable*. There is a third scenario where the solution does not converge to a steady state, but does not immediately show oscillations either. In these cases the deformation becomes large so the numerical code breaks down and we cannot tell whether they represent divergent or oscillatory instability.

5. Discussion

Flow limitation does occur in the parameter region investigated. The 'negative effort dependence' in our results in which the flow rate tends to zero as P_{ud} is increased, seems to be universal, unlike the flow limitation measured in tube experiments. This is probably due in part to the fact that we assume the same constant tension for each solution curve. This will not be true in a real experiment, since when the membrane is stretched more, the overall tension (even if assumed uniform along the membrane) would increase and, as shown in figure 13, the limited flow rate increases as tension increases. More important, probably, is the fact that the elastic restoring force in a tube arises in most circumstances from azimuthal stretching when the tube is dilated and bending when it is buckled (often represented by a 'tube law') and not primarily from longitudinal tension. However, 'negative effort dependence' has been observed in

tube flow (Gavriely *et al.* 1984; Gavriely & Grotberg 1988; Bertram & Castles 1999), and is present in a three-dimensional calculation when the full nonlinear shell theory for the elastic wall is taken into account (Heil & Pedley 1996; Heil 1997), although the degree of negative dependence is much smaller than in our case.

It is noted that all the points that are located on the first solution branch, parallel to the solution curve for Poiseuille flow, are stable. These are: A_1, B_1, C_1, C_5, D_1, D_4'. On the other hand, all the points located on the upper part of the second branch are unstable: e.g. B_2, B_3, C_2, C_5', D_2, D_4. These unstable modes can be either oscillatory or divergent. The most interesting points are those located on the lower part of the second branch, i.e. A_2, B_4, C_3, D_3, D_5, E_1, E_2. Solutions on this branch seem to be sensitive to which type of boundary condition is used. They can be stable for one type of boundary conditions but unstable for another and they can present self-excited oscillations or divergent instabilities, again depending on the boundary conditions. Points C_3 and E_2, for example, are stable for BC(III), but are unstable for BC(I) and BC(II). We note that BC(III) is the case for which the reference pressure is chosen at the downstream end, while BC(I) and BC(II) are the ones for which upstream pressure is chosen to be zero. As pointed out in a previous paper (Luo & Pedley 1998), these three cases are different mathematically and physically. BC(I) and BC(II) allow upstream flow rate to vary, and the BC(III) does not, for example. Also, the system with fixed upstream pressure may be intrinsically more complex and unstable than that with fixed upstream flow rate (and fixed downstream pressure). Such increased complexity was found even in a grossly oversimplified lumped-parameter model, because the governing ordinary differential equation was third order rather than second order (Bertram & Pedley 1982). Different stability behaviours are also observed by Pedrizzetti (1999) when the reference pressure or flow discharge is imposed upstream and then downstream of a tube with an elastic membrane insertion. We believe that this difference may be demonstrated with carefully controlled experiments.

It is worth interpreting the present results in terms of dynamical system or catastrophe theory. In our system, there are three independent control parameters, i.e. Re (or P_{ud}), P_{ue} (or P_{de}), and T, where either Re or P_{ud} can be seen as a state variable when the other one is used as a control parameter. Therefore, it is quite natural to see static bifurcations such as fold and cusp catastrophes in our system (Thompson 1982), as well as possibly bifurcations from infinity, as shown in Cases D and E.

As our system is non-conservative, dynamic bifurcations also occur. Self-excited oscillations may be one of the results of a dynamic bifurcation. Such bifurcations have been found in similar systems, such as a simply supported pipe carrying a flowing fluid which exhibits either divergence or oscillatory behaviour akin to flutter (Holmes 1977).

As was mentioned earlier, some of the solution curves in figure 5 represent a saddle–node bifurcation: the first branch of the solution curve has nodes which are stable, the upper part of the second branch which curves back has saddle points which give unstable solutions, and the lower part of the second branch has nodal points again though some of these solutions can be unstable (table 1). Such behaviour is commonly found in a number of dynamical systems (Golubitsky & Schueffer 1985). It should, however, be noted that our system is of infinite dimension, so direct comparisons with low-dimensional dynamical systems which are governed by ordinary differential equations can be only suggestive.

The stability test is not a rigorous one in the sense that the types of perturbation are limited. Some solutions may be stable to the perturbations described here, but may be unstable to different forms of perturbation. It would be interesting to carry out a

linear stability analysis of the system so that a comparison with the present results can be made. This would involve solving the Orr–Sommerfeld equations coupled to the linearized elastic membrane equation; such a study is under way.

The multiple solutions obtained here are not necessarily all the possible steady solutions of the system in the parameter space investigated. This is simply because the numerical code needs a good initial guess to be able to obtain a steady solution. Such an initial condition is not easy to obtain unless a thorough scan is performed in the three-dimensional space of control parameters, which would be prohibitively costly in computational resources, using the current approach.

Different values of the upstream and downstream rigid channel lengths, L_u and L_d , would have an influence on the instability of the steady solution and on the resulting unsteady solutions. This can be seen even in lumped-parameter models such as that of Pedley (1980, chapter 6). The effect of varying the downstream length L_d was briefly discussed in our previous study (Luo & Pedley 1996) where it was shown to have a quantitative but not a qualitative effect. However, in the present study, we limit ourselves to investigating cases with different values of Re (P_{ud}), T, and P_{ue} only, while values of L, L_u and L_d are fixed. This is mainly due to the extensive computing requirement, and the belief that L_u and L_d will have small qualitative effects. The reason that L is also fixed here is that we found in the corresponding one-dimensional analytical model (Luo & Pedley 1995) that L can be combined with T in a single dimensionless parameter $\lambda = L/\sqrt{T}$ (Luo & Pedley 1995). Extending this finding into two dimensions, we expect the effect of increasing L to be equivalent to that of reducing $\sqrt{T}$.

Two more points are worth mentioning. One is that if a solution is unstable for a fixed upstream flow rate and downstream pressure as in BC(III), then it is unstable for BC(I), where the upstream and downstream pressures are fixed while the flow rate is a variable, or BC(II), where the downstream flow rate is fixed, and the downstream pressure and upstream flow rate are variables. In other words, BC(III) is the most stable case in the three scenarios.

The other is that all the points located on the solution branch corresponding to flow limitation are unstable for fixed P_{ue} (BC(I),(II)), while some solutions in the flow limitation phase are stable for fixed P_{de} (BC(III)). Thus for the limited points of steady solutions investigated here, it seems that flow limitation is not always associated with the unstable steady solution, and hence self-excited oscillations. Interestingly, in a recent experiment on flow in thick-walled tubes it was also found that flow limitation is not always coupled with large-amplitude self-excited oscillations (Bertram & Castles 1999).

Flow separation is observed for all cases, whether the flow is limited or not, in which part of the membrane is collapsed and Re is high enough. It seems that there is no correlation between the development of flow separation and the occurrence of flow limitation or multiple solutions. Flow separation is also observed in the bulging case for high enough Reynolds number.

To establish the relationship between energy dissipation and the steady solutions, the rate of viscous energy dissipation per unit volume, $\Phi = (u_{i,j} + u_{j,i})^2/2Re$, is calculated at each point in the flow domain for the steady solutions. The contours of Φ are shown as darker curves in figure 10, and it can be seen that most of the energy dissipation is accumulated around the narrowest section. The detailed contribution of different parts of the flow domain can be estimated by integrating Φ over four different sections of the channel (with x in the ranges 5–9, 9–13, 13–17, 17–21, see Luo & Pedley 1996, 1998). When the membrane collapses, the first section roughly corresponds to the region in which most of the viscous dissipation occurs in the thin

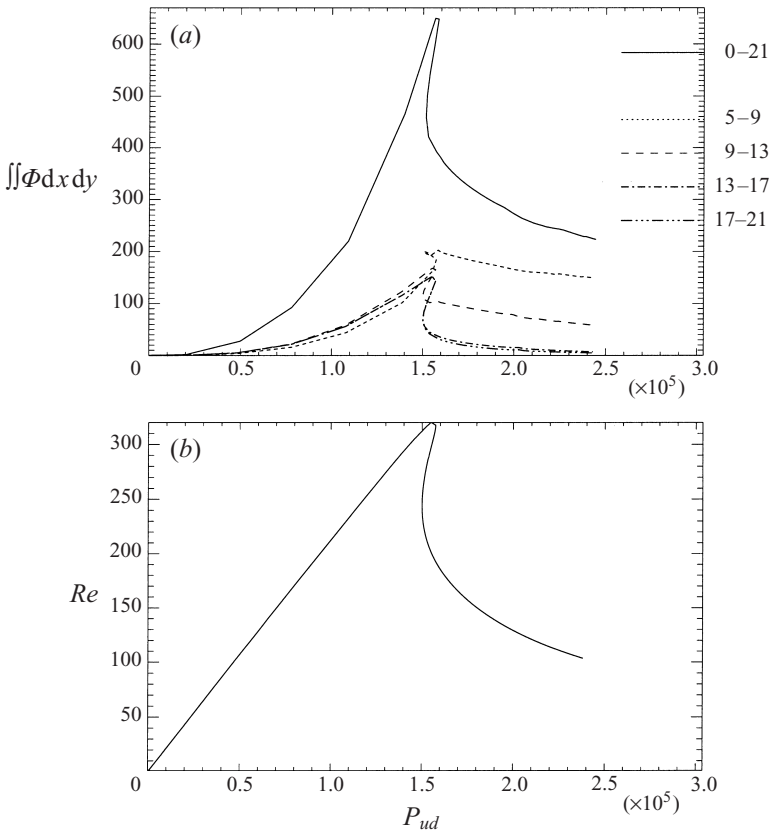

FIGURE 14. (*a*) Energy dissipation in Case B calculated for four sections along the channel, $x = 5$–9, 9–13, 13–17, 17–21, and (*b*) the corresponding Re, P_{ud} curve.

boundary layer that develops on each wall between $x = 5$ and the narrowest point; the second section accounts for the dissipation caused by the primary flow separation immediately after the narrowest point; and the third and fourth sections represent dissipation in the eddies that may be generated further downstream.

Although Φ has been calculated for all Cases A–E, only one graph for Case B ($P_{ue} = 0.27 \times 10^5$) is shown here in figure 14, since the main features are common to all the cases. First, we may note that Φ in all the four sections increases roughly proportionally with Reynolds number before the Re, P_{ud} curve reaches the turning point (first bifurcation), as in Poiseuille flow. However, once the curve turns, indicating that the flow is limited and the wall becomes collapsed, only sections 3 and 4 follow the drop of Reynolds number, while Φ in section 1 remains more or less constant after the turning point, and Φ in section 2 decreases a little after the turning point and then remains nearly constant. The value of Φ in section 2 is only about half of the value in section 1 during the flow limitation phase. This is consistent with the previous findings (Luo & Pedley 1996, 1998) that the thin boundary layers upstream of the narrowest point dissipate the largest portion of the viscous energy. The primary flow separation comes second. In Cases C and D, where the flow is not limited Φ simply becomes proportional to Re, the differences among the four sections remaining minor. It should be noted that in Case C, although the almost overlapped solution branches

have two distinct solutions (one is stable, the other is not), the energy dissipation in the two branches shows very little difference.

The fact that all the solution points located on the first solution branch before the bifurcations are stable suggests that a bulging wall configuration usually indicates a stable system. As emphasized previously (Kamm & Pedley 1989), oscillations are closely associated with energy dissipation, however caused. This explains why some one-dimensional models can produce self-excited oscillations regardless of whether the energy loss is based on flow separation (Jensen 1992) or friction only (Hayashi *et al.* 1998), as long as some kind of energy loss is included.

6. Conclusion

The results demonstrate flow limitation in that, as P_{ud} is increased, for a prescribed value of P_{ue} below a critical value P_c, Re first increases to a maximum and then smoothly decreases. However, for $P_{ue} > P_c$, there is a range of P_{ud} for which three steady solutions exist, indicating hysteresis in the flow limitation process and a sudden decrease in flow rate as P_{ud} passes its critical value at the top of that range (figure 5). As P_{ue} increases further, the range of P_{ud} for which multiple solutions are predicted increases rapidly, suggesting (counter-intuitively) that it should be possible to maintain stable, unlimited flow at high P_{ud}. Both P_{ue} and T are found to be crucial in generating the sequence of bifurcations in the solution branches.

The stability of the solutions is found to depend on the boundary conditions when the steady solution is perturbed. This is true especially for the flow limitation phase, when solutions can be stable if downstream pressure and upstream flow rate are fixed, but unstable if upstream pressure and downstream flow rate are fixed, or if both upstream and downstream pressure are kept constant (for the selected points tested here). However, using any of the three boundary conditions, the bulging solutions located in the unlimited flow phase are found to be stable.

We conclude that there is not a definite link between flow limitation and the instability of the steady solutions (and hence self-excited oscillations). However, some degree of collapse of the membrane is essential to destabilize the steady solutions, and in order to provide the energy loss needed for the generation of self-excited oscillations.

Special thanks are due to Drs C. Davies, M. Heil and J. B. Grotberg for helpful discussions and their suggestions. EPSRC is thanked for financial support, through grant No. GR/M07243 and through the award of a Senior Fellowship to T. J. Pedley. The QMW Engineering Faculty Funding to X. Y. Luo is also appreciated.

REFERENCES

Barkley, D. 1990 Theory and predictions for finite-amplitude waves in two-dimensional plane Poiseuille flow. *Phys. Fluids* A **2**, 955–970.

Bertram, C. D. 1986 Unstable equilibrium behaviour in collapsible tubes. *J. Biomechanics* **19**, 61–69.

Bertram, C. D. & Pedley, T. J. 1982 A mathematical model of unsteady collapsible tube behaviour. *J. Biomechanics* **15**, 39–50.

Bertram, C. D., Sheppeard, M. D. & Jensen, O. J. 1994 Prediction and measurement of the area-distance profile of collapsed tubes during self-excited oscillation. *J. Fluids Struct.* **8**, 637–660.

Bertram, C. D., & Castles, R. J. 1999 Flow limitation in uniform thick-walled collapsible tubes. *J. Fluids Struct.* **13**, 399–418.

Bonis, M. & Ribreau, C. 1978 Etude de quelques proprietes de l'ecoulement dans une conduite collabable. *La Houille Blanche* **3**/4, 165–173.

Brower, R. W. & Scholten, C. 1975 Experimental evidence on the mechanism for the instability of flow in collapsible vessels. *Trans. ASME: J. Biomech. Engng* **13**, 389–845.

Cancelli, C. & Pedley, T. J. 1985 A separated-flow model for collapsible-tube oscillations. *J. Fluid Mech.* **157**, 375–404.

Carpenter, P. W. & Garrad, A. D. 1986 The hydrodynamic stability of flow over Kramer-type compliant surfaces. Part 2. Flow-induced surface instabilities *J. Fluid Mech.* **170**, 199–232.

Carpenter, P. J. & Morris, P. J. 1990 The effect of anisotropic wall compliance on boundary-layer stability and transition, *J. Fluid Mech.* **218**, 171–223.

Conrad, W. A. 1969 Pressure-flow relationships in collapsible tubes. *IEEE Trans. Bio-Med. Engng* **BME-16**, 284–295.

Davies, C. & Carpenter, P. W. 1997*a* Numerical simulation of the evolution of Tollmien-Schlichting waves over finite compliant panels. *J. Fluid Mech.* **335**, 361–392.

Davies, C. & Carpenter, P. W. 1997*b* Instabilities in a plane channel flow between compliant walls. *J. Fluid Mech.* **352**, 205–243.

Elliott, E. A. & Dawson, S. V. 1977 Test wave speed theory of flow limitation in elastic tubes. *J. Appl. Physiol.* **43**, 516–522.

Gavriely, N., Palti, Y., Alroy, G., & Grotberg, J. B. 1984 Measurement and theory of wheezing breath sounds. *J. Appl. Physiol.* **57**, 481–492.

Gavriely, N. & Grotberg, J. B. 1988 Flow-limited and wheezes in a constant flow and volume lung preparation. *J. Appl. Physiol.* **64**, 17–20.

Gavriely, N., Shee, T. R., Cugell, D. W. & Grotberg, J. B. 1989 Flutter in flow-limited collapsible tubes: a mechanism for generation of wheezes. *J. Appl. Physiol.* **66**, 2251–2261.

Gresho, P. M., Lee, R. L. & Sani, R. L. 1979 On the time-dependent solutions of the Navier–Stokes equations in two and three dimension. In *Recent Advances in Numerical Methods in Fluids* (ed. C. Taylor & K. Morgan), Vol. 1, pp. 27–79.

Golubitsky, M. & Schueffer, D. 1985 *Singularities and Groups in Bifurcation Theory*, Vol. 1. Springer.

Grotberg, J. B. & Gavriely, N. 1989 Flutter in collapsible tubes: a theoretical model of wheezes. *J. Appl. Physiol.* **66**, 2262–2273.

Hayashi, S., Hayase, T. & Kawamura, H. 1998 Numerical analysis for stability and self-excited oscillation in collapsible tube flow. *Trans. ASME: J. Biomech. Engng* **120**, 468–475.

Heil, M. 1997 Stokes flow in collapsible tubes: computation and experiment. *J. Fluid Mech.* **353**, 285–312.

Heil, M. 1998 Stokes flow in an elastic tube – A large-displacement fluid-structure interaction problem. *Intl J. Numer. Meth. Fluids* **28**, 243–265.

Heil, M. & Pedley, T. J. 1996 Large post-buckling deformations of cylindrical shells conveying viscous flow. *J. Fluids Struct.* **10**, 565–599.

Holmes, P. 1977 Bifurcations to divergence and flutter in flow induced oscillations: a finite dimensional analysis. *J. Sound. Vib.* **53**, 471.

Hyatt, R. E., Schilder, D. P. & Fry, D. L. 1958 Relationship between maximum expiratory flow and degree of lung inflation. *J. Appl. Physiol.* **13**, 331–336.

Jensen, O. E. 1990 Instabilities of flow in a collapsed tube. *J. Fluid Mech.* **220**, 623–659.

Jensen, O. E. 1992 Chaotic oscillations in a simple collapsible tube model. *Trans. ASME: J. Biomech. Engng* **114**, 55–59.

Jensen, O. E. 1998 An asymptotic model of viscous flow limitation in a highly collapsed channel. *Trans. ASME: J. Biomech. Engng.* **120**, 544–546.

Jensen, O. E. & Pedley, T. J. 1989 The existence of steady flow in a collapsed tube. *J. Fluid Mech.* **206**, 339–374.

Kamm, R. D. & Pedley, T. J. 1989 Flow in collapsible tubes: A brief review. *Trans. ASME: J. Biomech. Engng* **111**, 177–179.

Lowe, T. W. & Pedley, T. J. 1996 Computation of Stokes flow in a channel with a collapsible segment. *J. Fluids Struct.* **9**, 885–905.

Luo, X. Y. & Pedley, T. J. 1995 Numerical simulation of steady flow in a 2-D collapsible channel. *J. Fluids Struct.* **9**, 149–197.

Luo, X. Y. & Pedley, T. J. 1996 Numerical simulation of unsteady flow in a 2-D collapsible channel. *J. Fluid Mech.* **314**, 191–225, and corrigendum, **324**, 408–409.

Luo, X. Y. & Pedley, T. J. 1998 The effects of the wall inertia on the 2-D collapsible channel flow. *J. Fluid Mech.* **363**, 253–280.

Matsuzaki, Y. & Matsumoto, T. 1989 Flow in a two-dimensional collapsible channel with rigid inlet and outlet. *Trans. ASME: J. Biomech. Engng* **111**, 180–184.

Pedley, T. J. 1980 *The Fluid Mechanics of Large Blood Vessels*. Cambridge University Press.

Pedley, T. J. & Luo, X. Y. 1998 Modelling flow and oscillations in collapsible tubes. *J. Theor. Comput. Fluid Dyn.* **10**, 277–294.

Pugh, J. D. & Saffman, P. G. 1988 Two-dimensional superharmonic stability of finite-amplitude waves in plane Poiseuille flow. *J. Fluid Mech.* **194**, 296–307.

Pedrizzetti, G. 1999 Fluid flow in a tube with an elastic membrane insertion. *J. Fluid Mech.* **375**, 39–64.

Rast, M. P. 1994 Simultaneous solution of the Navier–Stokes and elastic membrane equations by a finite-element method. *Intl J. Numer. Meth. Fluids* **19**, 1115–1135.

Riks, E. 1979 An incremental approach to the solution of snapping and bucking problems. *Intl J. Solids Structures* **15**, 529–551.

Ruschak, K. J. 1980 A method for incorporating free boundaries with surface tension in finite element fluid-flow simulators. *Intl J. Numer. Meth. Engng* **15**, 639–648.

Saito, H. & Scriven, L. E. 1981 Studying of coating flow by the finite element method. *J. Comput. Phys.* **42**, 53–76.

Shapiro, A. H. 1977 Steady flow in collapsible tubes. *Trans. ASME: J. Biomech. Engng* 126–147.

Silliman, W. J. 1979 Viscous film flows with contact lines. PhD Thesis, University of Minnesota.

Thompson, J. M. T. & Hunt, G. W. 1973 *A General Theory of Elastic Stability*. John Wiley & Sons.

Thompson, J. M. T. 1982 *Instabilities and catastrophes in science and engineering*. John Wiley & Sons.

Webster, P. M., Sawatzky, R. P., Hoffstein, V., Leblanc, R., Hinchey, J. M. & Sullivan, P. A. 1985 Wall motion in expiratory flow limitation: Choke and flutter. *J. Appl. Physiol.* **59**, 1304–1312.